



# On the influence of the asthenospheric flow on the tectonics and topography at a collision-subduction transition zones: Comparison with the eastern Tibetan margin



Pietro Sternai<sup>a,\*</sup>, Jean-Philippe Avouac<sup>a</sup>, Laurent Jolivet<sup>b</sup>, Claudio Faccenna<sup>c</sup>, Taras Gerya<sup>d</sup>, Thorsten Wolfgang Becker<sup>e</sup>, Armel Menant<sup>b</sup>

<sup>a</sup> Division of Geology and Planetary Sciences, California Institute of Technology, Pasadena, CA, USA

<sup>b</sup> Institute of Earth Sciences (ISTO) – University of Orléans, Orléans, France

<sup>c</sup> Department of Earth Sciences, University of Roma TRE, Rome, Italy

<sup>d</sup> Institute of Geophysics – Swiss Federal Institute of Technology (ETH), Zürich, Switzerland

<sup>e</sup> Department of Earth Sciences, University of Southern California, Los Angeles, USA

## ARTICLE INFO

### Article history:

Received 8 October 2015

Received in revised form 16 February 2016

Accepted 21 February 2016

Available online 27 February 2016

### Keywords:

Southeast Asia

Collision-subduction system

Asthenospheric flow

Extrusion tectonics

Topographic support

Geodynamic modeling

## ABSTRACT

The tectonic and topographic evolution of southeast Asia is attributed to the indentation of India into Eurasia, gravitational collapse of the uplifted terrains and the dynamics of the Sunda and other western Pacific subduction zones, but their relative contributions remain elusive. Here, we analyse 3D numerical geodynamic modelling results involving a collision-subduction system and show that vigorous asthenospheric flow due to differential along-strike slab kinematics may contribute to the surface strain and elevations at collision-subduction transition zones. We argue that protracted northward migration of the collisional front and Indian slab during south to south-westward rollback subduction along the Sunda margin might have produced a similar asthenospheric flow. This flow could have contributed to the southeast Asia extrusion tectonics and uplift of the terrains around the eastern Himalayan syntaxis and protruding from southeast Tibet. Therefore, we suggest that the tectonics and topographic growth east and south-east of Tibet are controlled not only by crustal and lithospheric deformation but also by asthenospheric dynamics.

© 2016 Elsevier Ltd. All rights reserved.

## 1. Introduction

The growth of the Tibetan plateau and the magnificent mountains of Asia has been long ascribed to lithospheric shortening and thickening along the India-Eurasia collisional margin (Argand, 1924), following the closure of the Tethyan ocean and on-going since ~50 Ma (Molnar and Tapponnier, 1975; Jolivet et al., 1990; Meyer et al., 1998; Cowgill et al., 2003). Unlike the abrupt Himalayan mountain front, the gentler but still impressive topography along the eastern margin of Tibet developed in a predominantly trans-tensional tectonic regime (Leloup et al., 1995; Wang et al., 1998; Hall and Morley, 2004). These fundamental observations and the geophysical evidence suggesting the presence of a weak lower crust below Tibet (Nelson et al., 1996; Xu et al., 2007) triggered a debate about the partitioning between clock-wise rigid

rotation (Tapponnier et al., 1982; Armijo et al., 1986; Avouac and Tapponnier, 1993; Leloup et al., 1995; Meade, 2007) or viscous eastward evacuation of the Eurasian crust and lithosphere, possibly involving crustal channel flow (England and Houseman, 1986; Royden et al., 1997; Clark and Royden, 2000; Clark et al., 2005; Schoenbohm et al., 2006; Copley and McKenzie, 2007; Royden et al., 2008). These models put different emphasis on strain localization, vertical gradients of strain due to depth-dependent rheologies, the role of gravitational body forces and tractions at the base of the lithosphere, and the influence of plate boundary dynamics. Unravelling the influence of these factors is challenging also because analyses based on the distribution of gravitational potential energy (GPE) (England and Molnar, 1997) or simplified mechanical models such as the thin viscous sheet (England and McKenzie, 1983) might provide limited insights (Lechman et al., 2011; Schmalholz et al., 2014).

Common to all proposed models are a focus on crustal dynamics and, regarding the effects of plate boundary dynamics, the assumption that subduction of oceanic lithosphere beneath eastern Eurasia and Indonesia chiefly created the accommodation space

\* Corresponding author at: Department of Earth Sciences, University of Cambridge, Cambridge, UK.

E-mail address: [psternai@caltech.edu](mailto:psternai@caltech.edu) (P. Sternai).

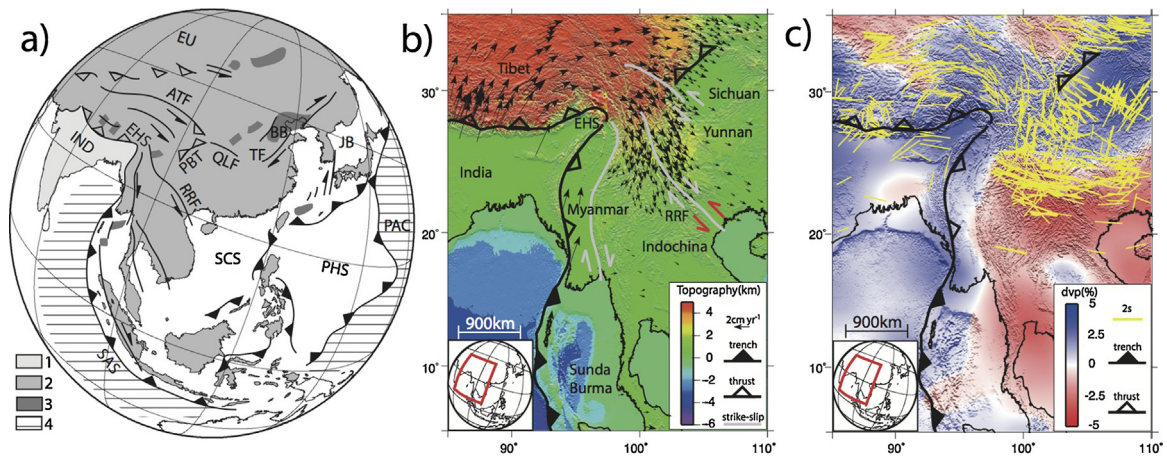


**Fig. 1.** (a) Tectonic map of southeast Asia and the Sunda and western Pacific subduction zones. 1: Indian (IND) continental plate; 2: Eurasian (EU) continental plate; 3: Actively opening intra-continental rifts; 4: Pacific (PAC) oceanic plate. AFT: Altyn Tagh Fault; BB: Bohai Basin; EHS: Eastern Himalayan Syntax; PBT: Pengguan and Beichuan Thrusts; PHS: Philippine Sea; QLS: Quin Ling Fault; RRF: Red River Fault; SAS: Sumatra-Andaman (Sunda) subduction; SCS: South China Sea; TF: Tanlu Fault. (b) Topography, GPS data (black arrows) from Wang et al. (2001), Zhang et al. (2004) and Gan et al. (2007) and major tectonic structures. Arrows along the strike-slip fault zones show the dominant sense of shear. Red and grey arrows along the Red River Fault differentiate between the sense of shear during the middle- and late-Cenozoic, respectively. (c) Average seismic wave velocity anomalies between 50 and 350 km depth from Schaeffer and Lebedev, 2013 and seismic anisotropies (green markers) from Wüstefeld et al. (2009). The low velocities beneath Tibet are due to its deep crustal root (which reaches to 80 km depth), while surface wave tomography suggests that a mantle lid with rather high seismic velocities underlies most of Tibet (Priestley et al., 2008). (For interpretation of the references to color in figure legend, the reader is referred to the web version of the article.)

for unconstrained continental extrusion. Some authors proposed that the suction exerted by these subduction zones could have contributed to regional extension and extrusion (Burchfiel and Royden, 1985; Jolivet et al., 1990, 1994; Northrup et al., 1995; Fournier et al., 2004; Flesch et al., 2005; Schellart and Lister, 2005; Ghosh et al., 2006; Royden et al., 2008). Concerning basal tractions, large-scale mantle convection might provide support to the topography of southeast Asia through vertical stresses (Ricard et al., 1993; Lithgow-Bertelloni and Gurnis, 1997) and contribute to the overall India-Eurasia convergence (Ghosh et al., 2008, 2009; Alvarez, 2010; Becker and Faccenna, 2011). Minor attention, however, has been given to the potential forcing from the asthenospheric return flow owing to protracted northward migration of the Indian slab and indentation front during rollback (late-Eocene to middle-Miocene) or stable (middle-Miocene to present) subduction along the Sunda and western Pacific margins (Tapponnier et al., 1986; van der Hilst and Seno, 1993; Hall and Morley, 2004; Sibuet et al., 2004; Honza et al., 2004; Royden et al., 2008; Replumaz et al., 2013) (shortened to “differential along-strike slab kinematics” or similar paraphrases in the following).

Our principal objective is thus to assess the potential role of the asthenospheric return flow in response to differential along-strike kinematics in affecting the surface tectonics and topography across coupled collision-subduction systems. To this aim, we present and discuss results from numerical experiments involving joint continental collision and ocean-continent subduction. The experiments suggest that vigorous mantle flow can arise from differential along-strike slab kinematics and contribute to the surface strain and topography at the collision-subduction transition zone by modulating the upper plate’s isostatic and dynamic balance. These results are consistent with first-order structural, geophysical and geomorphic observations from southeast Asia and build upon previously proposed models for the evolution of the eastern Tibetan margin, which are first summarized hereafter.

### 1.1. Tectonics and topography east and southeast of Tibet

Intracontinental deformation of Eurasia involved a gradually increasing region after the onset of continental collision with the Indian plate (Argand, 1924; Tapponnier and Molnar, 1977;

Tapponnier et al., 2001; Royden et al., 2008; Copley et al., 2010). While thrusting and topographic growth in southern Tibet and Himalayas started as early as Eocene times (Aikman et al., 2008; Gebelin et al., 2013), large fragments of the Eurasian lithosphere were extruded eastward out of the collision zone towards southeast Asia (Tapponnier et al., 1982, 1986; Replumaz and Tapponnier, 2003; Akciz et al., 2008) (Fig. 1a and b). Until activation of the Altyn-Tagh fault zone during the Oligocene, the Red River shear zone marked the northern boundary of the east-moving fragments (Tapponnier et al., 1986; Leloup et al., 1995; Wang et al., 1998; Replumaz and Tapponnier, 2003). High mantle temperatures inferred from alkali-rich magmatism between ~30 and 50 Ma (Holbig and Grove, 2008) may have enhanced continental extrusion, which occurred during rapid trench retreat and slab rollback along the Sunda and western Pacific oceanic subduction zones relative to the main collisional front and Indian slab (Tapponnier et al., 1986; Jolivet et al., 1990; van der Hilst and Seno, 1993; Jolivet et al., 1994; Fournier et al., 2004; Royden et al., 2008; Replumaz et al., 2013). Differential along-strike kinematics of the Tethyan and western Pacific slabs are implied by widespread early-Cenozoic extension within the upper plate lithosphere of Indonesia (Hall and Morley, 2004), Eocene-Oligocene extension in the South and East China Seas (Sibuet et al., 2004), and Oligocene to middle-Miocene extension in the Sea of Japan (Jolivet and Tamaki, 1992; Tamaki, 1992; Jolivet et al., 1994; Honza et al., 2004) (Fig. 1a). Fast extrusion of the Eurasian lithosphere along the eastern Tibetan plateau margin has slowed after ~15–20 Ma, when slab rollback along the Sunda and western Pacific margins also diminished or ended (van der Hilst and Seno, 1993). Similarly, backarc basin opening in the Sea of Japan stopped at 10–12 Ma when the Philippine Sea Plate had moved northward and the Eurasia-Pacific-Philippine Sea triple junction reached its present position (Jolivet et al., 1994). The history of subduction along the southeast Eurasian and western Pacific margins as well as lithospheric contrasts in the collision zone is also revealed by seismic tomography. Fast velocity anomalies are observed beneath southern Tibet and northern India (Fig. 1c) together with dipping positive perturbations associated with the Sunda and other western Pacific slabs, which penetrate into the mantle transition zone in multiple locations (Káráson and van der Hilst, 2000; Li et al., 2008a,b; Replumaz et al., 2013; Schaeffer and

Lebedev, 2013; Auer et al., 2014). Other significant regional positive anomalies are seen in the Sichuan basin and eastern Siberia craton, while beneath the rest of southeast Asia and between the Indian and Sunda slabs seismic velocities are anomalously low.

Eastward to southeastward continental extrusion is going on at present as indicated from the pattern of active faulting (e.g., Molnar and Tapponnier, 1975; Tapponnier and Molnar, 1977), although eastward extrusion of Tibet is partially absorbed by shortening in the Nan Shan and Qilian Shan (Meyer et al., 1998) and to a lesser degree in the Longmen Shan thrust (Burchfiel, 2004; Rongjun et al., 2007). GPS data relative to stable Eurasia (Gan et al., 2007) (Fig. 1b) show convergence along the India–Eurasia margin and a prominent clockwise rotation around the Eastern Himalayan Syntax (EHS), consistent with trench retreat and slab rollback in the Indo-Burman region (Hall and Morley, 2004). Differently from within the plateau, where uplift related to the early India–Eurasia collision raised terrains already above sea level (Murphy et al., 1997; Kapp et al., 2007), rapid uplift and erosion of relict low-relief terrains in eastern Tibet is coeval with the structural transition to the present-day kinematic pattern (Clark et al., 2006).

East–west extension in central and southern Tibet during the late Cenozoic (Armijo et al., 1986; Williams et al., 2001; Blisniuk et al., 2001; Zhang et al., 2004) is also ascribed to body forces due to high elevations (England and Houseman, 1986; England and Molnar, 1997; Flesch et al., 2001; Liu and Yang, 2003; Flesch et al., 2005). It is not clear, however, whether a gravitationally driven flow would coherently affect the deformation down to upper mantle levels or end within the crust, in turn implying intra-lithospheric rheological decoupling. Surface-wave tomography and receiver functions suggest the presence of a relatively weak lower crust confined along the eastern and southern plateau margin by rigid craton-like lithosphere beneath the Sichuan basin and the Indian plate, respectively (Nelson et al., 1996; Xu et al., 2007). Overall, the geometry of the plateau margins seems consistent with the underlying crustal rheology: the gently sloping north- and south-eastern plateau margin overlies a weak lower crust, while the steeper southern front overlies a strong crust throughout (Royden, 1996; Clark and Royden, 2000; Jordan and Watts, 2005). Rapid eastward flow in the deeper crust would explain relatively late uplift of the extruded terrains in the absence of crustal shortening.

## 1.2. Proposed models

Classical models of the India–Eurasia indentation involve plane horizontal strain of a plastic medium by a rigid indenter (Tapponnier et al., 1982; Peltzer and Tapponnier, 1988) or analogue experiments allowing for crustal thickening (Peltzer et al., 1982; Cobbold and Davy, 1988), which led to successful qualitative comparisons of the slip lines across the plastic medium to the orientations of major Asian strike-slip fault zones. Plane strain experiments, however, neglect the vertical deformation and therefore the topographic evolution and the forcing from surface elevation variations to the overall geometry of the deformation.

The regional lithospheric strain has been compared to numerical and analytical solutions of the deformation field within a thin viscous sheet (Bird and Piper, 1980; England and McKenzie, 1983; England et al., 1985; England and Houseman, 1986; Jiménez-Munt and Platt, 2006), a formulation that circumvents difficulties arising from the lack of knowledge on the crustal rock rheology by solving the 3D strain field for depth-averaged stresses or velocities. Jointly with the assumption of isostatic compensation this approach provided important insights amongst which are, for example, estimates of the average viscosity of the Tibetan lithosphere (England and Molnar, 1997) and quantifications of crust–mantle coupling and the contribution of the GPE or sub-lithospheric dynamics to the overall stress field (Flesch et al., 2001, 2005; Ghosh et al.,

2006; Copley et al., 2011). Yet, inferring a compensation depth where complex collisional and subduction dynamics altered the usual crust–mantle–asthenosphere stratification and imply vigorous sub-crustal motion is, at best, speculative. Moreover, neglecting depth-dependent behaviour across southeast Asia may be inappropriate if the lower crust beneath Tibet is weaker relative to the upper crust (Nelson et al., 1996; Xu et al., 2007). More recent models accounting for lower crustal channel flow relative to the upper crust have shown that depth-dependent rheological variations affect the surface strain and topography consistently with the observed surface structures and kinematics (Willett et al., 1993; Royden, 1996; Clark and Royden, 2000; Beaumont et al., 2004; Lechman et al., 2011; Capitanio, 2014; Capitanio et al., 2015). However, incomplete constraints on rheological variations of crustal and mantle rocks associated with changes of the chemical, thermal and pressure conditions at depth throughout the collisional and subduction history of the southeast Asia remain a substantial limitation for depth-dependent strain predictions. The relative contributions from each deformation mechanism to the total strain evolution remain elusive. Model formulations that account simultaneously for multiple deformation mechanisms are therefore desirable for the aim of quantitatively characterizing the overall deformation pattern or recognize additional potential contributions to the total strain.

## 2. Methods

In this section, we outline the modelling approach and the methods of analysis, while more details about the numerical solutions can be found in Gerya and Yuen (2007) and Gerya (2010). The setup and boundary conditions (Fig. 2) as well as the parametric study involving the numerical experiments discussed in this manuscript are also described in detail in Sternai et al. (2014), where we focused on extrusion dynamics rather than the forcing on the topography. Here, we report the aspects that are more relevant to this study, a summary of the material properties (Table 1) and videos showing the evolution of the reference model run (Videos S1–S4).

### 2.1. Numerical modelling approach and reference setup

We simulate the geodynamic evolution of a convergent collision–subduction system characterized by along-strike differential slab kinematics constrained by the wealth of observations from southeast Asia through self-consistent high-resolution 3D numerical thermo–mechanical modelling. We use the numerical model I3ELVIS to solve the 3D momentum, continuity and energy equations with the finite differences method, accounting for depth-dependent non-Newtonian visco-plastic crustal and mantle rheologies (Gerya, 2010). The numerical setup and boundary conditions of the reference model are specified in Fig. 2; additional simulations, whose setup is similar to that of the reference model (differences are mentioned explicitly), are described in Section 3.2. We imposed the upper plate crust as 35 km thick where  $z$  (i.e., the along-strike direction)  $\leq 490$  km and 45 km thick where  $z > 510$  km (linear interpolation in between). The initial thermal structure of all continental plates is laterally uniform with 0 °C at the surface and 1300 °C at 90, 140 and 150 km depth for the upper plate, indenter and backstop continent, respectively. The oceanic domain, characterized by a trench-parallel weak fracture zone to initiate subduction and a trench-perpendicular weak fracture zone to allow for slab tearing, separates the three continental plates. The thermal structure of the oceanic lithosphere is that of a half-space cooling age of 120 Ma (e.g., Turcotte and Schubert, 2002). Uniform and constant in time  $x$ -parallel velocities equal to  $\sim 2$  cm  $a^{-1}$  (convergence) are imposed to the  $x = 2000$  km boundary.

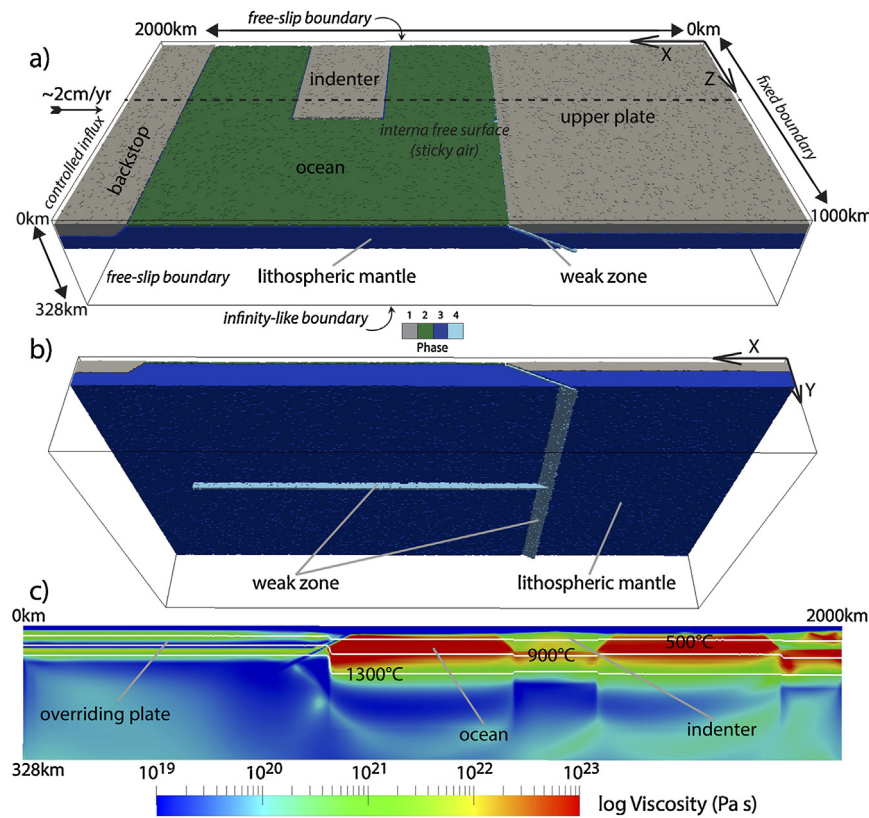


**Fig. 2.** 3D reference model setup with colours showing the initial rock type distribution: 1 – continental crust; 2 – oceanic crust; 3 – lithospheric mantle; 4 – hydrated/serpentinized mantle (initially imposed “weak fracture zone”). (b) Initial model domain and location of the “weak fracture zones” into the lithosphere to initialize subduction (z-parallel) and allow for differential along-strike slab kinematics as described in Sternai et al., 2014. Other phases in (a) and (b) are cut off for clarity. (c) x–y viscosity profile (location shown by the dashed line in (a)) of the initial model domain. Also shown in white are the initial 1300 °C, 900 °C and 500 °C isotherms. The velocity boundary conditions are free slip at the top (y = 0 km) and at both the front and back boundaries (z = 0 km and z = 1000 km). The left and right boundaries (x = 0 km and x = 2000 km) use constant x-parallel velocities, which define the material influx. Global mass conservation is ensured by material outflux through the lower permeable boundary (y = 328 km). The top surface of the lithosphere is calculated dynamically as an internal free surface through a 12 km thick layer of “sticky air” (Gerya, 2010). (For interpretation of the references to color in figure legend, the reader is referred to the web version of the article.)

Material properties, initially distributed on ~130 million randomly distributed Lagrangian markers, are advected through the marker-in-cell technique (e.g., Gerya, 2010) accordingly to the computed velocity field and a fourth-order Runge–Kutta scheme. Advected properties are then interpolated by weighted distance averaging on a regularly spaced Eulerian grid (501 by 165 by 197 nodes to discretize the 2000 by 328 by 1000 km model domain – i.e., resolution of ~4, 2 and 5 km – in the x, y and z dimension, respectively). This operation enables the integration of stresses or other parameter estimates (as described in the following section) to remain unaffected by numerical diffusion of sharp gradients.

Predictions from multi-layered numerical models are particularly affected by rheological parameters that cannot be measured directly (the limitation, however, is common to all formulations), but can be constrained by laboratory experiments (Ranalli, 1995) and observables (England et al., 1985; Baumann and Kaus, 2015). The ability to account simultaneously for multiple deformation mechanisms (i.e., thickening/thinning, buckling, viscous flow, etc.) and geodynamic processes (i.e., continental collision and ocean-continent subduction) and quantify their relative contributions to the overall strain and topographic evolution without being tied to depth-averaged values (as, for example, with thin viscous sheet-like models) enables to identify potential sub-crustal

**Table 1**

Qz. and Ol. correspond to the abbreviations of Quartzite and Olivine. k denotes the thermal conductivity,  $\rho_0$  is the density,  $C_p$  is the specific heat capacity,  $E_a$  is the activation energy,  $V_a$  is the activation volume, n is the stress exponent,  $\eta_0$  is the reference viscosity,  $H_r$  is the radiogenic heat production,  $\phi_{eff}$  is the effective internal friction angle. Cohesion is 1 MPa for each phase.

	$k$ (W m <sup>-1</sup> K <sup>-1</sup> )	$\rho_0$ (kg m <sup>-3</sup> )	$C_p$ (J kg <sup>-1</sup> K <sup>-1</sup> )	$E_a$ (kJ mol <sup>-1</sup> )	$V_a$ (cm <sup>3</sup> mol <sup>-1</sup> )	n	$\eta_0$ (Pa <sup>n</sup> s)	$H_r$ (mW m <sup>-3</sup> )	Material	sin( $\phi_{eff}$ )
Material properties										
Sticky-air	20	1	100	0	0	1	$1 \times 10^{19}$	0	Air	0
Water	20	1000	3330	0	0	1	$1 \times 10^{19}$	0	Water	0
Sediment	$0.64 + 807/(T+77)$	2600	1000	154	8	2.3	$1.97 \times 10^{17}$	2	Wet Qz.	0.15
Crust (upper plate, backstop)	$0.64 + 807/(T+77)$	2750	1000	154	8	2.3	$1.17 \times 10^{17}$	2	Wet Qz.	0.15
Crust (indenter)	$1.18 + 807/(T+77)$	2950	1000	238	8	3.2	$4.8 \times 10^{22}$	2	Wet Qz.	0.15
Oc. Crust	$1.18 + 474/(T+77)$	3000	1000	238	8	3.2	$4.8 \times 10^{22}$	0.25	Wet Qz.	0.15
Mantle	$0.73 + 1293/(T+77)$	3300	1000	532	8	3.5	$3.98 \times 10^{20}$	0.02	Dry Ol.	0.6
Weak Zone	$0.73 + 1293/(T+77)$	3300	1000	471	8	4	$5 \times 10^{20}$	0.05	Wet Ol.	0

forcing. Complex mantle–crustal interactions in collision or subduction systems, with several implications for the large-scale tectonics and topography, have been demonstrated through 2D multi-layered numerical models (Willett et al., 1993; Beaumont et al., 2004; Faccenda et al., 2009; Nikolaeva et al., 2010). Solving also for the lateral dimension provides us with the possibility to account for along-strike rheological variations, which are inescapable across coupled collision-subduction systems and established along, for instance, the India-Eurasia and Sunda margins. The focus is put on the potential contribution from the resulting asthenospheric return flow to the surface topography and tectonics at the collision-subduction transition zone. We compare the inferred tectonics and topography to those observed across southeast Asia during the Cenozoic and find a certain degree of similarity. However, a number of differences between our model setups and the natural setting can be readily recognized (e.g., uniform convergence velocity in space and time, somewhat smaller scale, simplification of the plate geometry, etc.) and we do not claim that our numerical model is representative of the entire subduction and collisional history of the India-Eurasia and Sunda margins. We further stress that assessments as to the causes of differential along-strike slab kinematics in southeast Asia are beyond the purpose of this study. As such, our work is primarily meant to test the hypothesis that asthenospheric dynamics across coupled collision-subduction systems can affect the surface evolution rather than produce a realistic representation of the Cenozoic history of the India-Eurasia and Sunda margins.

## 2.2. Analytical investigation of the numerical results

Results are analysed in terms of *GPE* and lithospheric strain and stress variations quantified through depth-integration (depth-integrated values are equal to depth-averaged values multiplied by the corresponding thickness) across the model domain. The force balance equation,  $\partial\sigma_{ij}/\partial x_j = -\rho g_i$ , where  $\sigma_{ij}$  is the total stress tensor,  $x_j$  is the  $j$ th coordinate axis,  $\rho$  is the density and  $g_i$  is the  $i$ th component of gravity, can be used to describe the deformation of a continuous lithosphere. In the above equation,  $i$  denotes  $x$ ,  $y$  and  $z$  coordinate axes and the repeated index  $j$  represents the summation over  $x$ ,  $y$  and  $z$  (we use a right-handed coordinate system where  $x$ ,  $y$  and  $z$  point south, down and east, respectively). If the horizontal length scale is large in comparison with the thickness of the lithosphere and local density and elevation contrasts are isostatically compensated, the force balance equation implies that

$$\sigma_{yy}(y) = -g \int_{s.t.}^y \rho(y') dy' \quad (1)$$

where *s.t.* stands for surface topography, stating that the weight per unit area of any column of rock is supported by the vertical normal stress on its base,  $\sigma_{yy}(y)$ . Depth-integration of Eq. (1) from the surface topography to the reference level (or compensation depth, given the assumption of isostatic equilibrium),  $L$ , leads to the definition of *GPE* as the negative depth-integrated vertical normal stress (Fleitout and Froidevaux, 1983)

$$\bar{\sigma}_{yy} = \int_{s.t.}^L (L-y)\rho(y)g dy = GPE \quad (2)$$

the over bar representing depth-integration. As previously described by e.g., England and McKenzie (1983), England and Molnar (1997), Flesch et al. (2001) or Ghosh et al. (2009), substituting into the horizontal (i.e.,  $x$ - $z$  plane) force balance equation the relationship  $\tau_{ij} = \sigma_{ij} - \delta_{ij}1/3\sigma_{kk}$  (where  $\tau_{ij}$  is the deviatoric stress tensor,  $\delta_{ij}$  is the Kronecker delta and  $1/3\sigma_{kk}$  is the negative of

pressure) and integrating at depth form the surface topography to the reference level  $L$  leads to

$$\begin{aligned} \partial\bar{\tau}_{xx}/\partial x - \partial\bar{\tau}_{yy}/\partial x + \partial\bar{\tau}_{xz}/\partial z &= -\partial\bar{\sigma}_{yy}/\partial x + \tau_{xy}(L) \\ \partial\bar{\tau}_{zx}/\partial x + \partial\bar{\tau}_{zz}/\partial z - \partial\bar{\tau}_{yy}/\partial z &= -\partial\bar{\sigma}_{yy}/\partial z + \tau_{zy}(L) \end{aligned} \quad (3)$$

Horizontal gradients of the depth-integrated deviatoric stress required to deform the lithosphere (i.e., the left-hand side of Eq. (3)) are balanced by horizontal gradients of *GPE* and the shear traction applied at the reference level by the underlying dynamics (i.e., the right-hand side of Eq. (3)).

We infer the contributions from crustal and sub-crustal dynamics to the surface evolution across the model domain by comparing the shear stress applied by the mantle flow associated with differential along-strike slab kinematics to the base of the crust and horizontal gradients of *GPE* determined by depth-integration throughout the crustal thickness (i.e., the reference level,  $L$ , corresponds to the base of the crust). This comparison also provides insights on the discrepancy between collisional strain pattern predictions assuming depth-independent behaviour and neglecting basal shear tractions (England and Houseman, 1986; England and Molnar, 1997) and those from a multi-layered rheology that accounts for the crustal and mantle dynamics arising from joint collision and subduction forcing. The choice of the base of the crust as reference level implies isostatic compensation at this depth. However, because vertical deviatoric traction arises from the mantle dynamics, a certain departure from the isostatic equilibrium is expected. The constitutive law

$$\tau_{ij} = H\hat{\epsilon}_{ij}^{1/n-1}\hat{\epsilon}_{ij} \quad (4)$$

where  $\hat{\epsilon} = 1/2((\partial v_i/\partial x_j) + (\partial v_j/\partial x_i))$  ( $v_{ij}$  being the velocity tensor) is the strain rate tensor,  $\hat{\epsilon}_{II} = \sqrt{1/2\hat{\epsilon}_{ij}\hat{\epsilon}_{ij}}$  is the second invariant of the strain rate tensor and  $H$  is a rheological coefficient, expresses the rheology of a “power law” fluid whose effective viscosity,  $\eta = 1/2H\hat{\epsilon}_{II}^{1/n-1}$ , is determined through experimental parameterization of common crustal and mantle rocks coefficients (Ranalli, 1995). The vertical deviatoric stress at depth,  $\tau_{yy}(y)$ , determined via Eq. (4), further elucidates the contribution from the sub-surface dynamics to the lithospheric strain and surface topography in terms of dynamic upward or downward deviatoric stress. Horizontal variations of  $\tau_{yy}(y)$  provide information on the degree of isostatic compensation and therefore on the suitability of the choice of base of the crust, or any other depth, as compensation depth.

As a post-processing operation, we apply the above analytical relationships to the values interpolated on the numerical Eulerian grid (i.e., after application of the fourth-order Runge–Kutta advection scheme). The *GPE*, in particular, is computed from such a discretized set of values as the depth-averaged vertical normal stress at nodes between (including those at) the surface topography and base of the crust multiplied by the corresponding crustal thickness. This provides a discrete bi-dimensional grid map of *GPE* values from which gradients in the  $x$  and  $z$  (i.e., horizontal) directions are derived. Horizontal *GPE* gradients are then compared to the shear stress as advected at the lowermost crustal Eulerian nodes.

## 2.3. Testing the analysis

As a test of our analysis, we consider a three-layer model configuration including lithospheric (crust and mantle lithosphere) and asthenospheric materials (Fig. 3a), based on experiments presented by Schmalholz et al. (2014). The horizontal boundary between the mantle and asthenosphere is at 120 km depth below the lowlands, and the asthenospheric layer extends to a depth of 200 km. While the top surface of the lithosphere is calculated as an internal free surface through a 15 km thick layer of “sticky air” and an “infinity-like” condition is applied to the bottom boundary (Gerya, 2010),

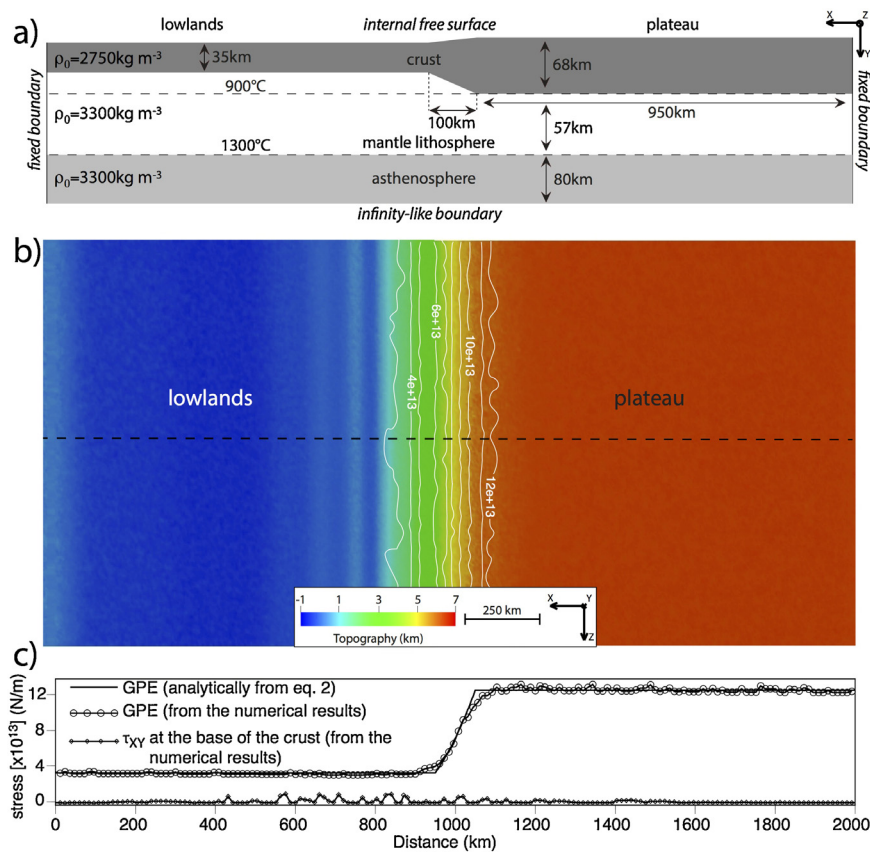


**Fig. 3.** (a)  $x$ – $y$  representation of the model setup of the test simulation following experiments described in Schmalholz et al. (2014) (parameters are the same along the  $z$ -axis).  $\rho_0$  is the material density. (b) Plan view of a selected time step (modelled time  $\sim 4$  Ma) of the test experiment showing the modelled topography (colours) and  $GPE$  (white isolines, units: N/m). (c) Profiles (the location is shown by the dashed line in (b)) of  $GPE$  calculated analytically from Eq. (2) and from the numerical results as well as  $\tau_{XY}$  at the base of the crust. (For interpretation of the references to color in figure legend, the reader is referred to the web version of the article.)

free-slip conditions are imposed on all lateral boundaries, which do not move (i.e., no imposed shortening or stretching).

Because this model is let to evolve under the only action of gravity, the flow and topography (Fig. 3b) within the model domain results only from lateral variations of  $GPE$  as dictated by the initial variations of the crustal thickness. Thus, the estimated  $GPE$  variations obtained by applying Eq. (2) to the set of discrete values on the numerical Eulerian grid (that we compare to the analytical solution of Eq. (2) in Fig. 3c) would explain the topography once the isostatic equilibrium is reached. This test also validates that, when shear tractions at the base of the crust (also shown in Fig. 3c) are negligible, the thin viscous sheet approximation reproduces reasonably well the dynamics of multi-layered numerical models, as previously pointed out by, for instance, Schmalholz et al. (2014).

### 3. Results

#### 3.1. Reference model

##### 3.1.1. Description of the numerical results

Like in southeast Asia, the geodynamic evolution of our model is characterized by pre-collisional oceanic subduction along the entire overriding plate margin, followed by simultaneous continental indentation and protracted subduction at the side of the collisional domain (Videos S1–S4). Increased buoyancy across a thicker portion of the overriding plate crust rise the surface topography to  $\sim 3$  km elevation prior to the onset of collision, which is in agreement with geological observations (Murphy et al., 1997; Kapp et al., 2007). The imposed crustal thickness variations result in a basal layer of partially molten, less viscous material below

the collisional margin, which is also consistent with observations (Nelson et al., 1996; Xu et al., 2007). Following the onset of continental indentation, a plateau with a similar morphology to that of the current eastern half of Tibet is generated through thrusting along the collisional domain (Figs. 1b and 4a). Syn-collisional continental extrusion towards the subduction zone takes place through trans-tensional deformation (Fig. 4b), with a resulting distribution of elevations across the collision–subduction transition zone to a first order comparable to that currently present east and southeast of Tibet (Fig. 1b and 4a).

At depth, an ascending/toroidal asthenospheric return flow develops below the upper plate and through the opening slab window triggered by the fast descent of the pre-collisional slab and enhanced by the increasing topographic weight during continental collision. The sub-collisional slab then hangs almost vertically during continental extrusion and rollback of the neighbouring slab (Fig. 4c). The rheological stratification of the upper continental plate is essentially unaffected by this early subduction event and the associated asthenospheric flow, thus tractions due to the mantle flow are imposed at the base of the lithosphere. The post-collisional ocean–continent subduction event is conditioned by the precedent flow of hot asthenosphere. The major effect is that the upwelling asthenosphere warmed the incipiently subducting lithosphere close to the slab tear, enhancing slab rollback and trench retreat and contributing to a further vigorous lateral/upwelling asthenospheric flow of up to  $\sim 12$  and  $\sim 9$   $\text{cm a}^{-1}$  in the horizontal and vertical direction, respectively, due to differential along-strike slab kinematics at the collision–subduction transition zone (Figs. 4 and 6). Such an asthenospheric flow is able to thermally erode the upper plate mantle lithosphere below the

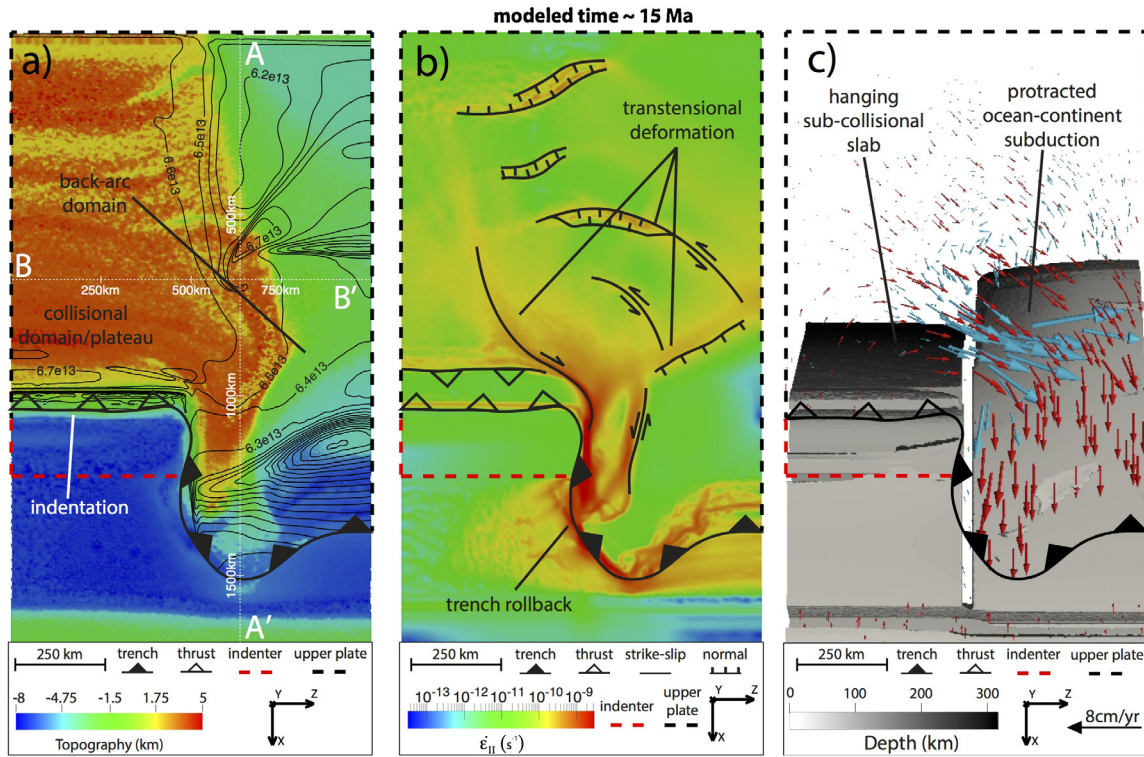


**Fig. 4.** Plan view of a selected time step (modelled time  $\sim 15$  Ma) of the numerical experiment showing (a) the modelled topography (colours) and  $GPE$  (black isolines, units:  $N/m$ ) distribution, (b) the second invariant of the rate-of-strain tensor and major tectonic structures and (c) the slab geometry (visualized through an iso-viscosity surface equal to  $10^{23}$  Pa s, colour-coded by depth) and the velocity field in the crust (red arrows) and asthenosphere (blue arrows). The major subduction/thrust fronts are also shown in each panel. Dashed red and black lines represent the continental indenter and upper plate boundaries, respectively. The white dotted lines in (a) show the location of the profiles in Fig. 7. (For interpretation of the references to color in figure legend, the reader is referred to the web version of the article.)

back-arc extensional domain. During advanced stages of the model run, the rheological stratification of the upper plate in the back-arc extensional domain is thus characterized by the absence of a rigid lithospheric mantle, which translates into shear stresses of up to  $\sim 100$  MPa applied directly to the base of the crust by the asthenospheric flow (Fig. 7a and b).

Amongst the many limitations that our reference model is subject to, probably the most important is that free-slip back and front boundaries imply a symmetric collision-subduction setting, while the India-Eurasia-Sunda-Western Pacific setting is inherently asymmetric, with major subduction zones and predominant extrusion towards the east. However, at the stage of the model run shown by, for instance, Fig. 4, a rotational trajectory of the surface particles around the collision-subduction transition zone is the only possible given that the continental indenter prevents the material from moving parallel to the  $x$ -axis in the collisional domain, forcing the flow towards the extending back-arc domain. An imposed influx or outflux across the  $z = 0$  km or  $z = 1000$  km boundaries would modify the geometry of such rotational motion thereby better reproducing, at least to some extent, the natural complexity. However, in this context, we favour a simplifying approach in which this additional complexity is neglected.

### 3.1.2. Results from the analytical investigation

As should be expected if the regional instantaneous deformation follows Eqs. (1)–(4),  $GPE$  from our numerical model reaches the highest magnitude in the plateau and gradually decrease across the collision-subduction transition zone to reach minimum values in the back-arc extensional domain (Fig. 4a). There is, however, a significant discrepancy between the topographic and  $GPE$  gradients across the extruded terrains arising because of the deviatoric shear tractions applied by the mantle flow to the base of the crust

and the simplifying assumption of isostatic compensation at this depth. We show in Figs. 5 and 7a, b that horizontal  $GPE$  gradients and deviatoric shear stresses at the base of the crust are similar in magnitude across both the plateau proper, the plateau margins and the extruded terrains. They therefore exert a similar control on the overall surface strain and elevations. Also noteworthy is that higher basal shear stresses (and horizontal  $GPE$  gradients) are found towards the plateau margins and in the back arc domain, where the most topographic changes in space and time are expected, while they assume relatively low values beneath the elevated terrains (Fig. 5). High basal shear stresses at the plateau margins imply a mechanical coupling between the crust and mantle and an active contribution from the mantle flow to the crustal deformation. Similar mantle and crustal (especially lower crustal) flow patterns below the plateau proper and across the extruded terrains (Fig. 6a) associated with relatively low basal shear stresses (Fig. 5) suggest that these layers flow jointly in response to a common driver: differential along strike slab kinematics.

The fit between predictions of topography from our model and those assuming isostatic equilibrium and approximating the lithosphere to a uniform viscous sheet with an average density of  $\sim 3000$   $kg/m^3$  is minimized for compensation depths of  $\sim 150$  km or higher, but still shows considerable differences (Fig. 7c and d, see the blue and red profiles). A similar outcome arises from the comparison between the topography predicted by our multi-layered model (i.e., accounting for the static and dynamic contributions to the surface elevations) and the isostatically-balanced topography resulting from the inferred lithospheric and asthenospheric structures,  $Y_{iso} = ((\rho_a - \rho_c)/\rho_a)l_c + ((\rho_a - \rho_m)/\rho_a)l_m$  where  $\rho_c$ ,  $\rho_m$  and  $\rho_a$  are the average crustal, mantle lithosphere and asthenospheric densities, respectively, and  $l_c$  and  $l_m$  are the crustal and mantle thickness (Fig. 7c and d see the blue and green profiles). In both

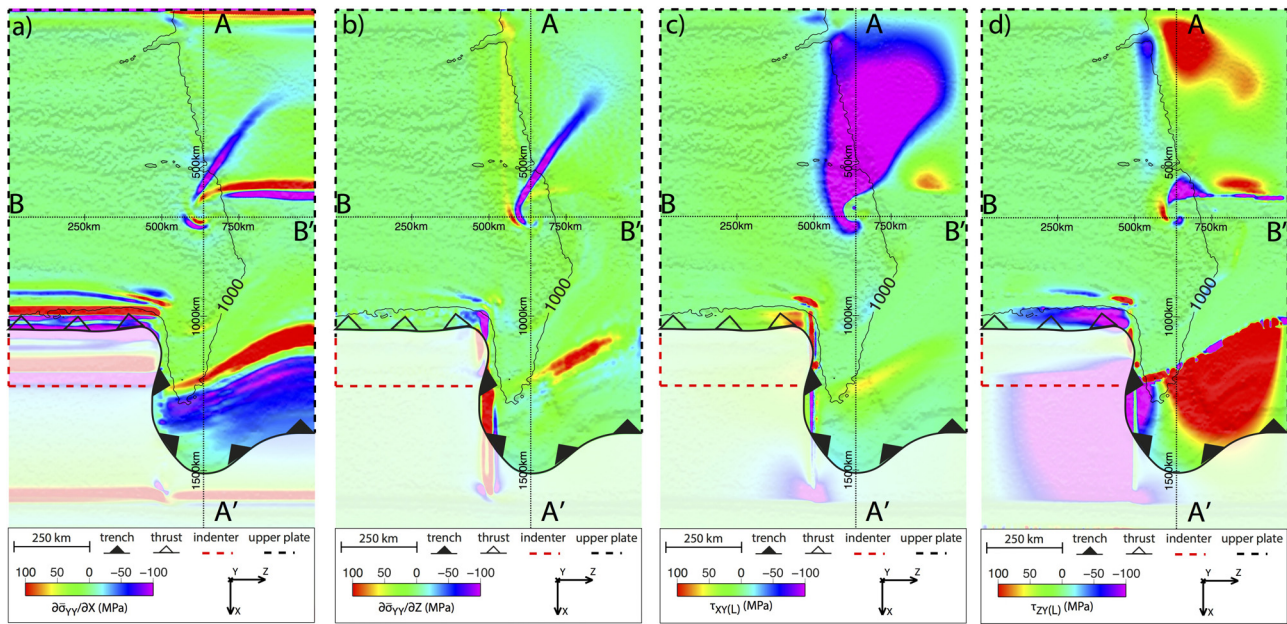


**Fig. 5.** Plan view of a selected time step (same as Fig. 4) showing (a)  $\partial\sigma_{yy}/\partial x$ , (b)  $\partial\sigma_{yy}/\partial z$ , (c)  $\tau_{xy}(L)$ , (d)  $\tau_{zy}(L)$ . Note that these quantities vary between the same order of magnitude, suggesting that horizontal gradients of GPE (i.e.,  $\partial\sigma_{yy}/\partial x$  and  $\partial\sigma_{yy}/\partial z$ ) and deviatoric shear stresses at the base of the crust ( $\tau_{xy}(L)$  and  $\tau_{zy}(L)$ ) jointly contribute to the surface strain and elevation variations. Major subduction/thrust fronts are also shown in each panel. Dashed red and black lines represent the continental indenter and upper plate boundaries, respectively. Also shown in black is the 1000 m topographic elevation isoline. (For interpretation of the references to color in figure legend, the reader is referred to the web version of the article.)

cases, an overall agreement between elevation predictions in the plateau and a considerable discrepancy between the topographic estimates across the extruded terrains and in the proximity of the subduction zone can be observed, suggesting that dynamic contributions to the surface elevations outside of the collisional domain cannot be neglected.

In our numerical experiment, continental extrusion is enhanced by the suction exerted by self-consistent slab rollback in the subduction domain and, to a minor extent, by the imposed convergence. The balance between these driving factors and the resulting forcing from the asthenospheric flow to the horizontal crustal strain (that we do not investigate here, but have been addressed in Sternai et al., 2014) determines whether continental extrusion is accompanied by surface extension or shortening. In both cases the horizontal crustal velocity field is characterized by rotational trajectories (rigid dislocation or viscous flow of the upper and lower crust, respectively) with low angle to the lateral asthenospheric return flow generated by differential along-strike slab kinematics at the collision-subduction transition zone (Figs. 4c and 6a). The suction exerted by subduction of the oceanic mantle lithosphere, however, implies an upwelling component of motion in the asthenospheric return flow and a down-welling component of motion in the overriding plate lower crust across the extruded terrains, resulting in a modification of the initial rheological stratification due to thermal erosion and delamination of the upper plate mantle lithosphere (Fig. 6). In Fig. 6b, we also show that, unlike in the collisional domain where deviatoric upward stresses responsible for the plateau uplift are ascribed to upper crustal levels, the upwelling asthenosphere provides most of the upward deviatoric traction supporting the topography of the extruded terrains.

### 3.2. The role of convergence velocity, crustal thickness and geothermal gradient

We performed an additional numerical experiment with  $x$ -parallel velocities imposed to the  $x=2000$  km boundary of  $\sim 6$  cm  $a^{-1}$  (i.e., three time faster convergence rates than those of

the reference model). While the overall geodynamic evolution (i.e., pre-collisional oceanic subduction along the entire overriding plate margin, subsequent continental indentation and protracted subduction) is similar to that of the reference model, the principal effect of increased convergence velocities is that of reducing slab rollback and trench retreat (Fig. 8), as also recognized by previous studies (e.g., Schellart, 2005). The amount of upper plate extension and the asthenospheric return flow are thus reduced compared to those in the reference model at similar modelled times. As expected, because the asthenospheric forcing on the surface strain is reduced, GPE and topographic trends across the upper plate are similar.

Nikolaeva and co-workers presented an extensive investigation of the parameters that codetermine the initiation and evolution of an ocean-continent subduction on a 2D version of the numerical model used in this study (Nikolaeva et al., 2010). They found that increased thickness of the upper plate crust enhances subduction rates and leads to a faster geodynamic evolution. On the contrary, an increased upper plate lithospheric thickness leads to slower subduction rates and overall evolution. In the light of this previous work, we ran an additional simulation in which the initial 1300 °C isotherm is at 70 km (i.e., 20 km higher than in the reference model) depth and the crust measures 30 km where  $z \leq 490$  km and 40 km where  $z > 510$  km, with linear interpolation in between (i.e., 5 km thinner than in the reference model). Again, the overall geodynamic evolution is similar to that of the reference model, but some differences in the timing and amount of surface strain can be recognized (Fig. 9). A warmer lithosphere implies particularly fast slab rollback and asthenospheric return flow (Nikolaeva et al., 2010) while a thinner crust implies an overall lower topography across the upper plate. As a result, the amount of upper plate extrusion and trench retreat is larger than in the reference model at similar modelled times. A particularly fast asthenospheric return flow (Fig. 9c) produces similar effects on the upper plate strain and topography to those observed in the reference model (Fig. 4). Also noteworthy is that the amount of strike-slip deformation dominates on normal faulting in a warmer environment characterized by a thinner crust.

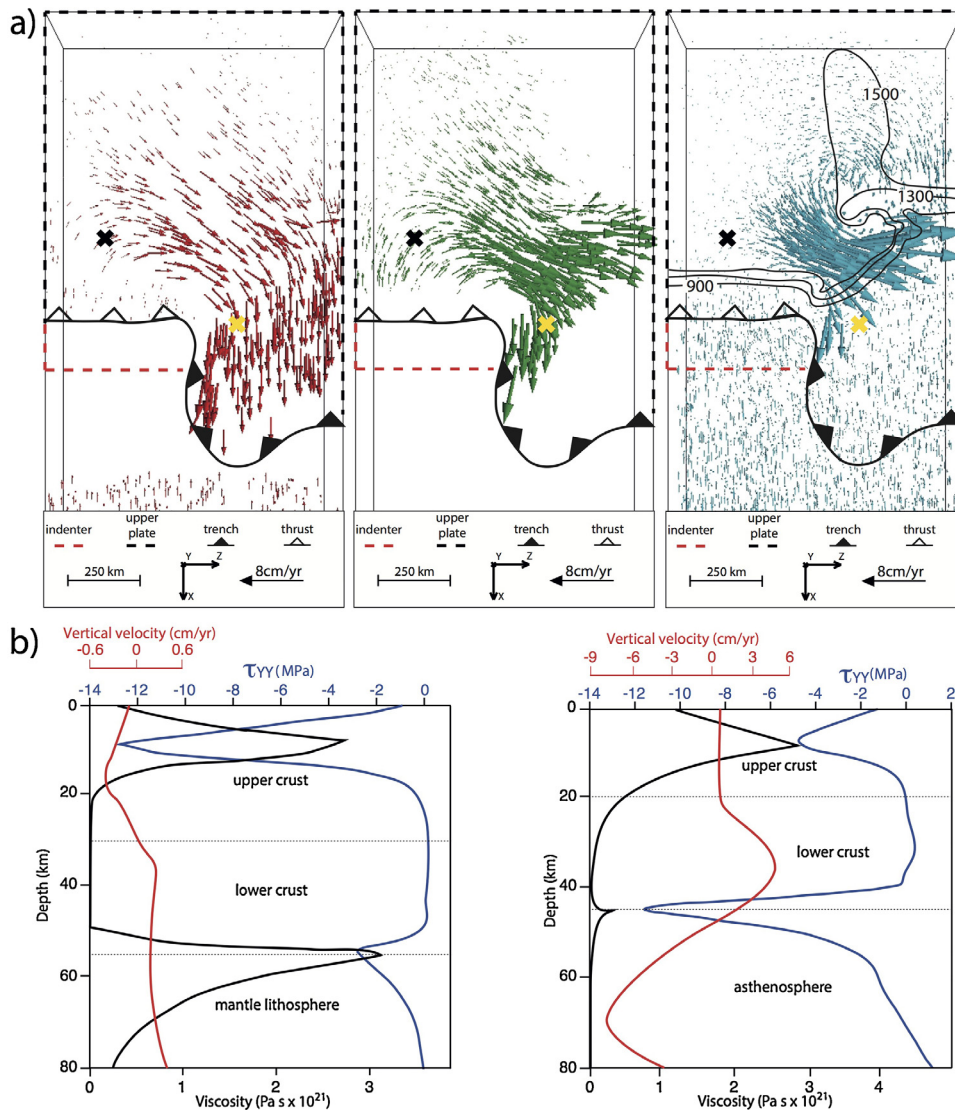


**Fig. 6.** (a) Plan view of a selected time step (same as Figs. 4 and 5) showing the velocity field within the upper crust (left panel, red arrows), lower crust (central panel, green arrows) and asthenosphere (right panel, blue arrows). The thermal anomaly produced by the asthenospheric return flow in response to differential along-strike slab kinematics and responsible for thermal erosion of the overriding plate mantle lithosphere beneath the extruded terrains is shown on the right panel by the 1500 °C, 1300 °C and 900 °C isotherms at 100 km depth (black solid lines). (b) Vertical velocity (red), vertical deviatoric stress (blue) and viscosity (black) profiles at depth. Black (left panel) and yellow (right panel) crosses in (a) show the profile location. Horizontal dotted lines show the rheological stratification. Note the absence of mantle lithosphere to decouple the lower crust and asthenosphere and higher deviatoric upward stresses to an asthenospheric level in the profile within the extruded terrains (right panel). (For interpretation of the references to color in figure legend, the reader is referred to the web version of the article.)

#### 4. Discussion and implications

A considerable discrepancy between horizontal *GPE* gradients and topography across southeast Asia (England and Molnar, 1997), to a first order comparable to our model predictions (Fig. 4a), questions isostatic equilibrium outside Tibet. Dynamic contributions to the regional elevations in eastern Tibet and Yunnan have been ascribed to an eastward flow in a mid-crustal channel below Tibet diverted to the north and south by the stronger Sichuan craton (Clark and Royden, 2000; Clark et al., 2005) and can, to some extent, explain this discrepancy. This interpretation, however, neglects relatively short wavelengths (i.e., a few hundred kilometres) gravity perturbations (Jin et al., 1994; Balmino et al., 2011) suggesting the presence of mass anomalies, in addition to the dynamic flow, involved in the support of the topography. Because the crust along portions of south-eastern Tibet has been stretching since at least ~4 Ma (possibly for more than 10 Ma locally) (Williams et al., 2001; Blisniuk et al., 2001; Zhang et al., 2004; Meade, 2007; Royden et al.,

2008) and several detachment-like extensional faults and back-arc basins, unlikely related solely to gravitational collapse, can be observed in the Indochina, Yunnan, Sunda and east China provinces, one may assume that the Sunda and western Pacific subduction zones provided an active contribution to southeast Asian tectonics from the Eocene to the present (Jolivet et al., 1990; van der Hilst and Seno, 1993; Leloup et al., 1995; Northrup et al., 1995; Jolivet et al., 1999; Jolivet et al., 2001; Fournier et al., 2004; Hall and Morley, 2004; Schellart and Lister, 2005). An alternative interpretation may, therefore, involve the lateral/upwelling asthenospheric return flow in response to northward motion of the Indian slab during south-to south-westward rollback or stable subduction along the Sunda region throughout the Cenozoic (Fig. 10).

The asthenospheric flow generated by differential along-strike slab kinematics, consistent with relatively short wavelengths gravity anomalies across the Eurasian plate (Jin et al., 1994; Balmino et al., 2011), may provide support to the topography of the upper plate by modulating the isostatic balance and applying dynamic

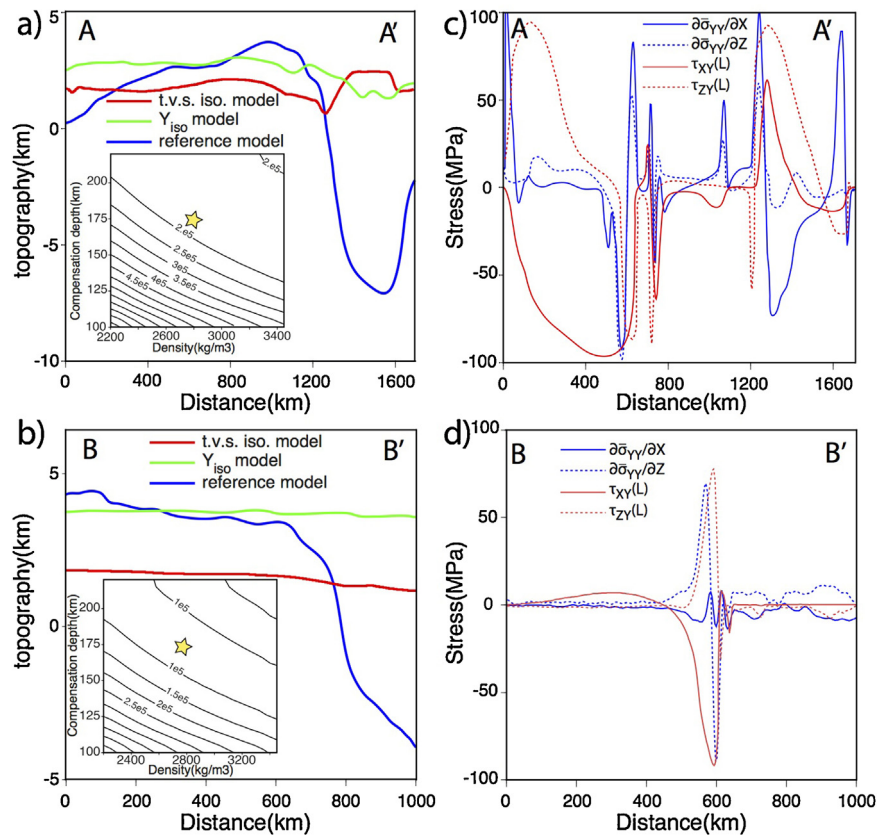


**Fig. 7.** (a, b) Topographic profiles (location is shown in Fig. 4a) from our model (blue line), assuming isostatic equilibrium and approximating the lithosphere to a uniform thin viscous sheet (shortened to t.v.s. in the caption) with an imposed average density (red line), and assuming isostatic equilibrium but accounting for the density and lithospheric structure from our model (i.e.,  $Y_{iso}$ , green line). The inset shows the  $L^2$ -norm distance (i.e., fit integrated along the profile) between blue and red profiles for different imposed density and compensation depth values. The star shows the pair value used for the general plot. (c, d) Profiles (same location as (a, b)) of the horizontal GPE gradients (i.e.,  $\partial\sigma_{yy}/\partial X$  and  $\partial\sigma_{yy}/\partial Z$ , blue lines) and deviatoric shear stress at the base of the crust (i.e.,  $\tau_{xy}(L)$  and  $\tau_{zy}(L)$ , red lines). Note that these quantities vary between the same order of magnitude, suggesting that they jointly contribute to the surface strain and elevation variations. (For interpretation of the references to color in figure legend, the reader is referred to the web version of the article.)

upward deviatoric stresses (Figs. 4–7). Consistently with this view, tomographic models show negative anomalies in seismic waves velocity across southeast Asia (Káráson and van der Hilst, 2000; Li et al., 2008a,b; Replumaz et al., 2013; Schaeffer and Lebedev, 2013; Auer et al., 2014) suggesting the presence of hot asthenospheric material at relatively low depths (Fig. 1c). In addition, the absence of foredeep basins of Cenozoic age along the eastern margin of the plateau (Royden et al., 1997, 2008), very low crustal seismic velocities (Meltzer et al., 1998; Yang et al., 2010), rapid exhumation and high-temperature metamorphism of Pleistocene age (Burg et al., 1997, 1998; Liu and Zhong, 1997) suggest a shallow brittle-ductile transition and rapid advection through a primary flow path into the massifs from depth rather than a shallow detachment related to lower crustal flow. Extreme exhumation rates, in particular, have been related to either exceptionally high rates of rock uplift owing to crustal-scale buckling (Burg et al., 1998) or a positive feedback among erosion, heat advection, rock strength and deformation (Zeitler et al., 2001). Recent chronological constraints and reconstructions of the former Yarlung-Tsangpo valley bottom (Wang et al., 2014), however, relate high erosion rates to rapid tectonic rock uplift and disprove any effective erosional control to the tectonic deformation. Based on our numerical results (Figs. 4–7), we propose that the asthenospheric return flow in response to along-strike differential slab kinematics across the collision-subduction transition contributes to such a tectonic upward push and sustains here the high strain rates and topography. Noteworthy is that accounting for surface processes in our experiment would lead to a coupling between erosion and crustal deformation (Aouac and

Burov, 1996; Zeitler et al., 2001), in turn enhancing localized rapid uplift along the edge of the plateau as well as in the syntax region.

Testing further our modelling results by comparing predictions with seismic anisotropy (Fig. 1c), currently the only technique at hand offering insights on the mantle strain, is beyond our possibilities for it would require accounting for the elastic tensor during deformation in order to convert the computed strain field into seismic anisotropy. However, an overall consistency between the crustal strain and seismic anisotropy in south-eastern Tibet has been interpreted to indicate coupling between mantle and crustal flow (Sol et al., 2007) (Fig. 6a). This observation does not necessarily rule out the presence of a weaker lower crust relative to the upper crust, but suggests that the lower crust is strong enough to transmit to upper crustal levels the stress arising from the mantle dynamics. In particular, previous investigations based on the thin viscous sheet formulation (Ghosh et al., 2006, 2009) demonstrate that deviatoric stresses at the base of the lithosphere from large-scale mantle convection contribute as much as those related to GPE gradients to the style and magnitude of the deformation worldwide, especially if the viscosity contrast between the asthenosphere and the lithosphere is between  $10^2$  and  $10^4$  (Ghosh et al., 2008). Accounting for a multi-layered rheology, our model shows that non-negligible deviatoric stresses also arise from more local mantle dynamics (Figs. 4–7). The effectiveness of these stresses is locally improved in our model by removal of the upper plate mantle lithosphere, in which case a viscosity contrast between the asthenosphere and the lower crust of 10–100 at  $\sim 40$ –60 km depth (Fig. 6b) is sufficient to produce deviatoric stresses comparable to those associated

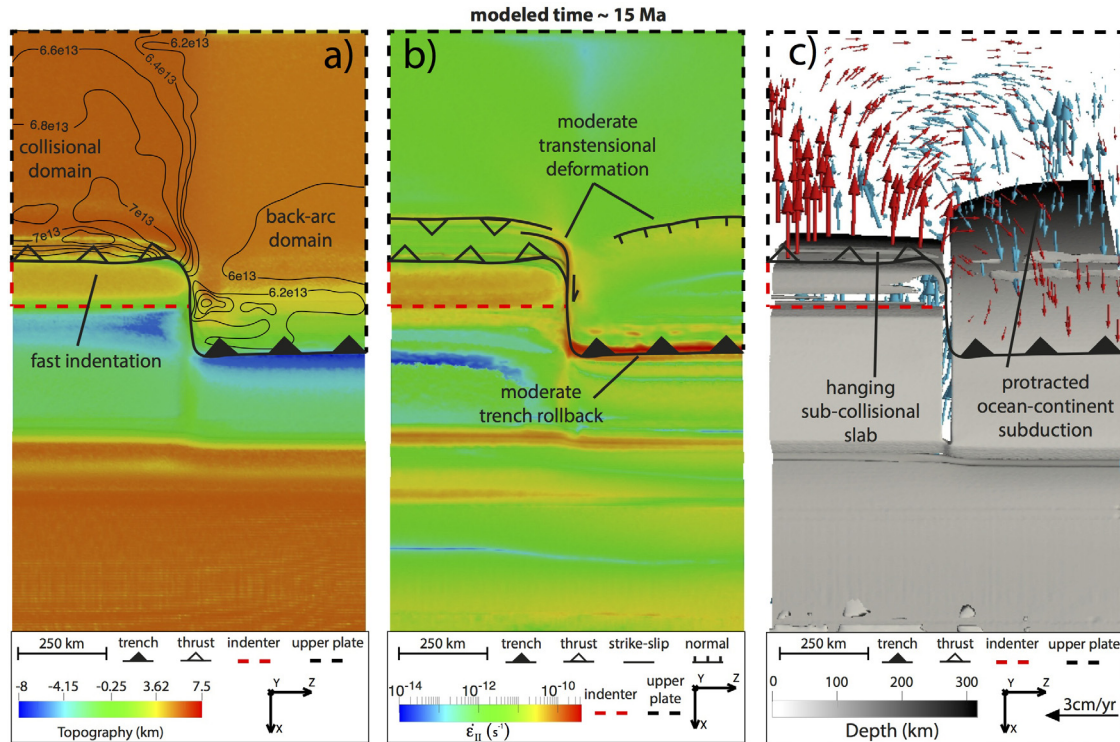


**Fig. 8.** Plan view of a selected time step (modelled time ~15 Ma) of a numerical experiment similar to the reference model (Fig. 4) but with faster convergence rates ( $\sim 6 \text{ cm a}^{-1}$ ). The figure is showing (a) the modelled topography (colours) and GPE (black isolines, units: N/m) distribution, (b) the second invariant of the rate-of-strain tensor and major tectonic structures and (c) the slab geometry (visualized through an iso-viscosity surface equal to  $10^{23}$  Pa s, colour-coded by depth) and the velocity field in the crust (red arrows) and asthenosphere (blue arrows). The major subduction/thrust fronts are also shown in each panel. Dashed red and black lines represent the continental indenter and upper plate boundaries, respectively. (For interpretation of the references to color in figure legend, the reader is referred to the web version of the article.)

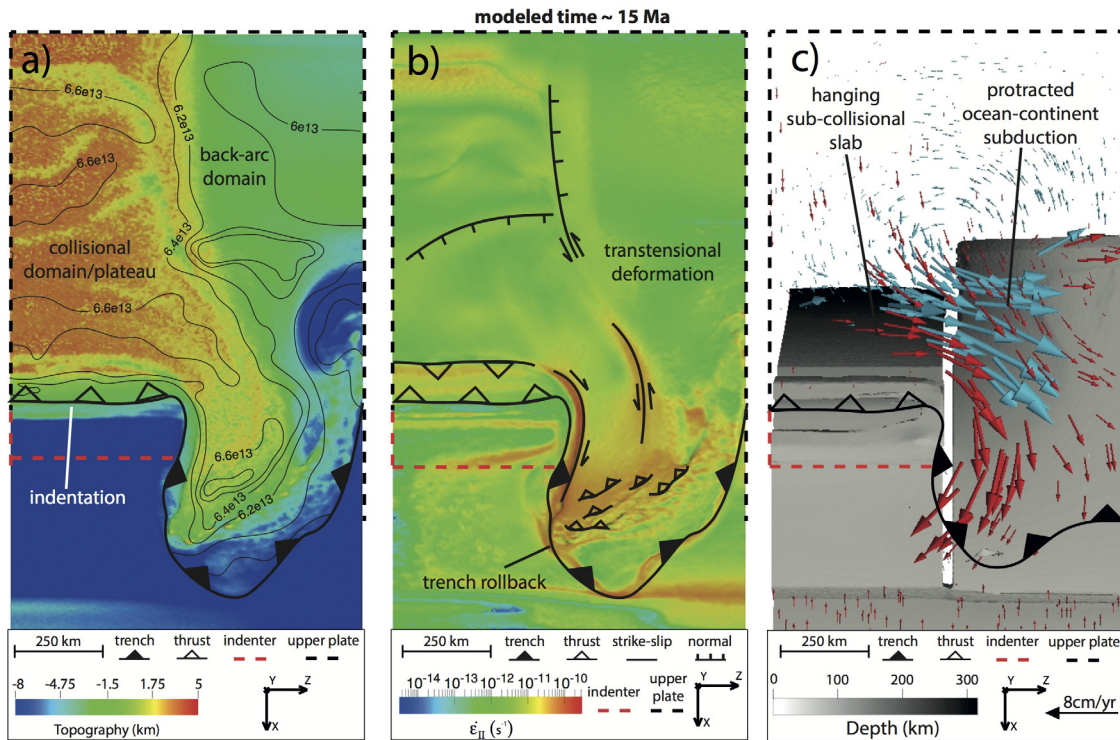


**Fig. 9.** Plan view of a selected time step (modelled time ~15 Ma) of a numerical experiment similar to the reference model (Fig. 4) but with different crustal and lithospheric thickness (see text for details). The figure is showing (a) the modelled topography (colours) and GPE (black isolines, units: N/m) distribution, (b) the second invariant of the rate-of-strain tensor and major tectonic structures and (c) the slab geometry (visualized through an iso-viscosity surface equal to  $10^{23}$  Pa s, colour-coded by depth) and the velocity field in the crust (red arrows) and asthenosphere (blue arrows). The major subduction/thrust fronts are also shown in each panel. Dashed red and black lines represent the continental indenter and upper plate boundaries, respectively. (For interpretation of the references to color in figure legend, the reader is referred to the web version of the article.)

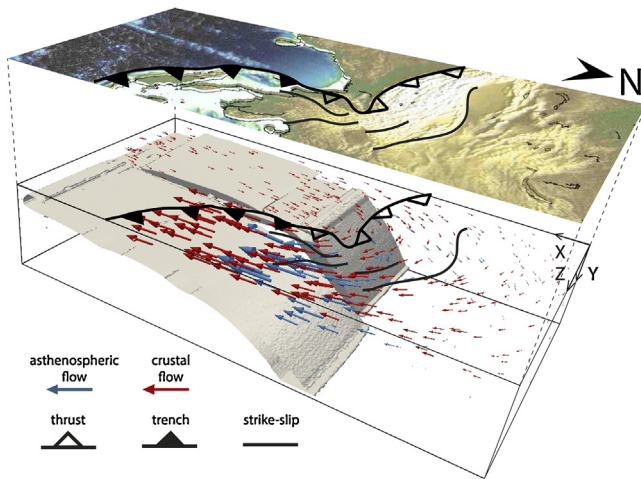


**Fig. 10.** Schematic representation of the proposed sub-crustal forcing to the surface tectonics and topography of the southeast Asia (note that the aim here is to facilitate comprehension by providing the readers with a visual representation of the proposed forcing and no physical meaning is implied by this figure). The present-day topography is joined to our modelling results (a different model time step with respect to that shown in Fig. 4 is displayed here) showing a possible representation of the overall geodynamics during the Cenozoic. The slab is visualized through an iso-viscosity surface equal to  $10^{23}$  Pa s, while red and blue arrows show the crustal and asthenospheric velocity field, respectively. The present-day location of the main strike-slip fault zones and collisional/subduction front is also shown in black and reported on the model results. (For interpretation of the references to color in figure legend, the reader is referred to the web version of the article.)

with horizontal *GPE* gradients (Figs. 5 and 7b, c). Long-wavelength traction fields to the base of the Indian plate generated by large-scale mantle convection due to subducted lithosphere are thought to foster the northward motion of India into Eurasia (Ghosh et al., 2009; Alvarez, 2010; Becker and Faccenna, 2011) but the opposite view, i.e., that basal traction might resist plate motion, has been advocated as well (Copley et al., 2010). In any case, more local asthenospheric dynamics may also influence the surface tectonics and topography across southeast Asia (Fig. 10), where long-lived collision-subduction dynamics likely altered the natural lithospheric rheological stratification.

Consistently with our numerical results, most Precambrian collisional orogens formed atop of warmer mantle relative to the Cenozoic and involved high topographies owing to protracted deformation over long periods (varying broadly between 50 and 200 Ma) with homogeneous thickening by mass redistribution in the upper and lower crust (Taylor and McLennan, 1995; Windley, 1995; Nironen, 1997; Cagnard et al., 2006; Gerya, 2014). We thus speculate that the geodynamic significance of crustal deformation and topographic growth driven by the asthenospheric flow is not peculiar to recent times, but also finds expression in Precambrian orogenesis.

## 5. Conclusions

In conclusion, several aspects related to the deformation and topographic evolution east and southeast of Tibet appear consistent with a forcing from the asthenospheric return flow owing to differential slab kinematics across the collision-subduction transition zone, a contribution that was neglected by previous models. While our experiment might exaggerate the influence of the asthenospheric flow on the lithospheric deformation, especially if compared to the present-day, the comparison between the observed and modelled surface kinematics is striking (Figs. 1, 4 and 6). There is, in addition, geological evidence that the early phase of extrusion of Indochina was affected by differential

along-strike slab kinematics and the associated mantle return flow. Such a mantle forcing is a non-exclusive alternative to previously proposed causes of deformation and is untie to unrealistic assumptions such as those of depth-independent behaviour, total isostatic compensation at crustal depths or a uniform and unaltered lithospheric rheological stratification despite long-evolving coupled collision-subduction dynamics. More comprehensive models of southeast Asia geodynamics, and continental dynamics in general, should therefore account for sub-crustal dynamics.

## Acknowledgements

We thank the California Institute of Technology and the University of Cambridge for support. We are also grateful to Boris Kaus, Ana M. Negredo and Wouter Schellart for thorough and very constructive revisions.

## Appendix A. Supplementary data

Supplementary data associated with this article can be found, in the online version, at <http://dx.doi.org/10.1016/j.jog.2016.02.009>.

## References

- Aikman, A.B., Harrison, T.M., Lin, D., 2008. Evidence for early (>44 Ma) Himalayan crustal thickening, Tethyan Himalaya, southeastern Tibet. *Earth Planet. Sci. Lett.* 274 (1–2), 14–23.
- Akiz, S., Burchfiel, B.C., Crowley, J., Jiyun, Y., Liangzhong, C., 2008. Geometry, kinematics, and regional significance of the Chong Shan shear zone, Eastern Himalayan Syntaxis Yunnan, China. *Geosphere* 4 (1), 292–314.
- Alvarez, W., 2010. Protracted continental collisions argue for continental plates driven by basal traction. *Earth Planet. Sci. Lett.* 296, 434–442.
- Argand, E., 1924. La tectonique de l'Asie. In: *Conférence faite à Bruxelles*.
- Armijo, R., Tapponnier, P., Tonglin, H., 1986. Late Cenozoic right-lateral strike-slip faulting in southern Tibet. *J. Geophys. Res.: Solid Earth Planets* 94 (B3), 2787–2838.
- Auer, L., Boschi, L., Becker, T.W., Nissen-Meyer, T., Giardini, D., 2014. Savani: a variable resolution whole-mantle model of anisotropic shear velocity variations based on multiple data sets. *J. Geophys. Res.* 119 (4).
- Avouac, J.P., Burrov, E.B., 1996. Erosion as a driving mechanism of intracontinental mountain growth. *J. Geophys. Res.* 101, 17–747.
- Avouac, J.P., Tapponnier, P., 1993. Kinematic model of active deformation in central Asia. *Geophys. Res. Lett.* 10, 895–898.
- Balmino, G., Vales, N., Bonvalot, S., Briais, A., 2011. Spherical harmonic modelling to ultra-high degree of Bouguer and isostatic anomalies. *J. Geodesy*, <http://dx.doi.org/10.1007/s00190-011-0533-4>.
- Baumann, T.S., Kaus, B.J., 2015. Geodynamic inversion to constrain the non-linear rheology of the lithosphere. *Geophys. J. Int.* 202 (2), 1289–1316.
- Beaumont, C., Jamieson, R.A., Nguyen, M.H., Medvedev, S., 2004. Crustal channel flows: 1. Numerical models with applications to the tectonics of the Himalayan-Tibetan orogen. *J. Geophys. Res.: Solid Earth* 109 (B6).
- Becker, T., Faccenna, C., 2011. Mantle conveyor beneath the Tethyan collisional belt. *Earth Planet. Sci. Lett.* 310, 453–461.
- Bird, P., Piper, K., 1980. Plane-stress finite-element models of tectonic flow in southern California. *Phys. Earth Planet. Inter.* 21 (2), 158–175.
- Blisniuk, P.M., Hacker, B.R., Glodny, J., Ratschbacher, L., Bi, S., Wu, Z., et al., 2001. Normal faulting in central Tibet since at least 13.5 Myr ago. *Nature* 412 (6847), 628–632.
- Burchfiel, B.C., 2004. New technology; new geological challenges. *GSA Today* 14 (4).
- Burchfiel, B.C., Royden, L.H., 1985. North-south extension within the convergent Himalayan region. *Geology* 13 (10).
- Burg, J.P., Davy, P., Nievergelt, P., Oberli, F., Seward, D., Diao, Z., Meier, 1997. Exhumation during crustal folding in the Namche Barwa syntaxis. *Terra Nova* 9, 117–123.
- Burg, J.P., Nievergelt, P., Oberli, F., Seward, D., Davy, P., Maurin, J.C., Diao, Z., Meier, M., 1998. The Namche-Barwa syntaxis: evidence for exhumation related to compressional crustal folding. *J. Asian Earth Sci.* 16, 3905–3927.
- Cagnard, F., Durrieu, N., Gapais, D., Brun, J.P., Ehlers, C., 2006. Crustal thickening and lateral flow during compression of hot lithospheres, with particular reference to Precambrian times. *Terra Nova* 18, 72–78.
- Capitanio, F., 2014. The dynamics of extrusion tectonics: insights from numerical modeling. *Tectonics* 33, 2361–2381.
- Capitanio, F.A., Replumaz, A., Riel, N., 2015. Reconciling subduction dynamics during Tethys closure with large-scale Asian tectonics: insights from numerical modeling. *Geochem. Geophys. Geosys.* (in press).
- Clark, M.K., Bush, J.W., Royden, H.R., 2005. Dynamic topography produced by lower crustal flow against rheological strength heterogeneities bordering the Tibetan Plateau. *Gephys. J. Int.* 162, 575–590.

- Clark, M., Royden, L., 2000. Topographic Ooze: building the eastern margin of Tibet by lower crustal flow. *Geology* 28 (8), 703–706.
- Clark, M.K., Royden, L.H., Whipple, K.X., Burchfiel, B.C., Zhang, X., Tang, W., 2006. Use of a regional, relict landscape to measure vertical deformation of the eastern Tibetan Plateau. *J. Geophys. Res.: Earth Surf.* 111 (F3).
- Cobbold, P.R., Davy, P.H., 1988. Indentation tectonics in nature and experiment. 2. Central Asia. *Bull. Geol. Inst. Univ. Uppsala* 14, 143–162.
- Copley, A., Avouac, J.P., Royer, J.Y., 2010. India-Asia collision and the Cenozoic slowdown of the Indian plate: implications for the forces driving plate motions. *J. Geophys. Res.: Solid Earth* 115 (B3).
- Copley, A., Avouac, J.P., Wernicke, B.P., 2011. Evidence for mechanical coupling and strong Indian lower crust beneath southern Tibet. *Nature* 472.
- Copley, A., McKenzie, D., 2007. Models of crustal flow in the India-Asia collision zone. *Geophys. J. Int.* 169 (2), 683–698.
- Cowgill, E., Yin, A., Harrison, T.M., Xiao-Feng, W., 2003. Reconstruction of the Altyn Tagh fault based on U–Pb geochronology: role of back thrusts, mantle sutures, and heterogeneous crustal strength in forming the Tibetan Plateau. *J. Geophys. Res.: Solid Earth* 108 (B7).
- England, P., Houseman, G., 1986. Finite strain calculations of continental deformation: 2. Comparison with the India-Asia collision zone. *J. Geophys. Res.: Solid Earth* 91 (B3), 3664–3676.
- England, P., Houseman, G., Sonder, L., 1985. Length scales for continental deformation in convergent, divergent, and strike-slip environments: analytical and approximate solutions for a thin viscous sheet model. *J. Geophys. Res.: Solid Earth* 90 (B5), 3551–3557.
- England, P., McKenzie, D., 1983. A thin viscous sheet model for continental deformation. *Geophys. J. Int.* 70 (2), 295–321.
- England, P., Molnar, P., 1997. Active deformation of Asia: from kinematics to dynamics. *Science* 278 (5338), 647–650.
- Faccenda, M., Minelli, G., Gerya, T.V., 2009. Coupled and decoupled regimes of continental collision: numerical modeling. *Earth Planet. Sci. Lett.* 278 (3), 337–349.
- Fleitout, L., Froidevaux, C., 1983. Tectonic stresses in the lithosphere. *Tectonics* 2, 315–324.
- Flesch, L.M., Haines, A.J., Holt, W.E., 2001. Dynamics of the India-Eurasia collision zone. *J. Geophys. Res.: Solid Earth* 106 (B8), 16435–16460.
- Flesch, L.M., Holt, W.E., Silver, P.G., Stephenson, M., Wang, C.Y., Chan, W.W., 2005. Constraining the extent of crust-mantle coupling in central Asia using GPS, geologic and shear wave splitting data. *Earth Planet. Sci. Lett.* 238, 248–268.
- Fournier, M., Jolivet, L., Davy, P., Thomas, J., 2004. Backarc extension and collision: an experimental approach to the tectonics of Asia. *Geophys. J. Int.* 157 (2), 871–889.
- Gan, W., Zhang, P., Shen, Z., Niu, Z., Wang, M., Wan, Y., Zhou, D., Cheng, J., 2007. Present day crustal motion within the Tibetan Plateau inferred from GPS measurements. *J. Geophys. Res.* 113.
- Gebelin, A., Mulch, A., Teyssier, C., Jessup, M.J., Law, R.D., Brunel, M., 2013. The Miocene elevation of Mount Everest. *Geology* 41 (7), 799–802.
- Gerya, T., 2010. Introduction to Numerical Geodynamic Modelling. Cambridge University Press.
- Gerya, T.V., 2014. Precambrian geodynamics: concepts and models. *Gondwana Res.* 25 (2), 442–463.
- Gerya, T., Yuen, D., 2007. Robust characteristics method for modelling multiphase visco-elasto-plastic thermo-mechanical problems. *Phys. Earth Planet. Int.* 163, 83–105.
- Ghosh, A., Holt, W.E., Flesch, L.M., 2009. Contribution of gravitational potential energy differences to the global stress field. *Geophys. J. Int.* 179 (2), 787–812.
- Ghosh, A., Holt, W.E., Flesch, L.M., Haines, A.J., 2006. Gravitational potential energy of the Tibetan Plateau and the forces driving the Indian plate. *Geology* 34 (5).
- Ghosh, A., Holt, W.E., Wen, L., Haines, A.J., Flesch, L.M., 2008. Joint modeling of lithosphere and mantle dynamics elucidating lithosphere-mantle coupling. *Geophys. Res. Lett.* 35 (16).
- Hall, R., Morley, C.K., 2004. Sundaland basins. In: *Continent-Ocean Interactions Within East Asian Marginal Seas.*, pp. 55–85.
- Holbig, E.S., Grove, T.L., 2008. Mantle melting beneath the Tibetan Plateau: experimental constraints on ultrapotassic magmatism. *J. Geophys. Res.: Solid Earth* 113 (B4).
- Honza, E., Tokuyama, H., Soh, W., 2004. Formation of the Japan and Kuril Basins in the Late Tertiary. In: *Continent-Ocean Interactions Within East Asian Marginal Seas.*, pp. 87–108.
- Jiménez-Munt, I., Platt, J.P., 2006. Influence of mantle dynamics on the topographic evolution of the Tibetan Plateau: results from numerical modeling. *Tectonics* 25 (6).
- Jin, Y., McNutt, M.K., Zhu, Y., 1994. Evidence from gravity and topography data for folding of Tibet. *Nature* 371, 669–674.
- Jolivet, L., Beyssac, O., Goffé, B., Avigad, D., Lepvrier, C., 2001. Oligo-Miocene midcrustal subhorizontal shear zone. *Tectonics* 20 (1), 46–57.
- Jolivet, L., Davy, P., Cobbold, P., 1990. Right-lateral shear along the Northwest Pacific Margin and the India-Eurasia Collision. *Tectonics* 9 (6), 1409–1419.
- Jolivet, L., Faccenna, C., D'Agostino, N., Fournier, M., Worrall, D., 1999. The kinematics of back-arc basins, examples from the Tyrrhenian, Aegean and Japan Seas. *Geol. Soc. Lond. Spec. Publ.* 164 (1), 21–53.
- Jolivet, L., Tamaki, K., 1992. Neogene kinematics in the Japan Sea region and volcanic activity of the northeast Japan Arc. *Proc. ODP Sci. Results* 127/128, 1311–1331.
- Jolivet, L., Tamaki, K., Fournier, M., 1994. Japan Sea, opening history and mechanism, a synthesis. *J. Geophys. Res.* 99, 22237–22259.
- Jordan, T.A., Watts, A.B., 2005. Gravity anomalies, flexure and the elastic thickness structure of the India-Eurasia collisional system. *Earth Planet. Sci. Lett.* 236, 732–750.
- Káráson, H., van der Hilst, R.D., 2000. Constraints on mantle convection from seismic tomography. In: *The History and Dynamics of Global Plate Motions.*, pp. 277–288.
- Kapp, P., DeCelles, P.G., Gehrels, G.E., Heizler, M., Ding, L., 2007. Geological records of the Lhasa-Qiangtang and Indo-Asian collisions in the Nima area of central Tibet. *Geol. Soc. Am. Bull.* 119 (7–8), 917–933.
- Lechman, S.M., May, D.A., Kaus, B.J., Schmalholz, S.M., 2011. Comparing thin-sheet models with 3-D multilayer models for continental collision. *Geophys. J. Int.* 187, 10–33.
- Leloup, P.H., Lacassin, R., Tapponnier, P., Scharer, U., Zhong, D., Liu, X., Zhang, L., Ji, S., Phan, T.T., 1995. The Ailao Shan-Red River shear zone (Yunnan, China), tertiary transform boundary of Indochina. *Tectonophysics* 251, 3–84.
- Lithgow-Bertelloni, C., Gurnis, M., 1997. Cenozoic subsidence and uplift of continents from time-varying dynamic topography. *Geology* 25 (8), 735–738.
- Liu, M., Yang, Y., 2003. Extensional collapse of the Tibetan Plateau: results of three-dimensional finite element modeling. *J. Geophys. Res.: Solid Earth* 108 (B8).
- Liu, Y.D., Zhong, D.J., 1997. Petrology of high-pressure granulites from the eastern Himalayan syntaxis. *Metamorph. Geol.* 15, 451–466.
- Li, C., van der Hilst, R., Engdahl, E.R., Burdick, S., 2008a. A new global model for P wave speed variations in Earth's mantle. *Geochim. Geophys. Geosyst.* 9, 5.
- Li, C., van der Hilst, R.D., Meltzer, A.S., Engdahl, E.R., 2008b. Subduction of the Indian lithosphere beneath the Tibetan Plateau and Burma. *Earth Planet. Sci. Lett.* 274 (1), 157–168.
- Meade, B.J., 2007. Present-day kinematics at the India-Asia collision zone. *Geology* 35 (1), 81–84.
- Meltzer, A.S., Sarker, G.L., SEeber, L., Armbruster, J., 1998. Snap, crackle, pop! seismicity and crustal structure at Nanga Parbat, Pakistan, Himalaya. *EOS* 79, F909.
- Meyer, B., Tapponnier, P., Bourjot, L., Métivier, F., Gaudemer, Y., Peltzer, G., Shunmin, G., Zhitai, C., 1998. Crustal thickening in Gansu-Qinghai, lithospheric mantle subduction, and oblique, strike-slip controlled growth of the Tibet plateau. *Geophys. J. Int.* 135 (1), 1–47.
- Molnar, P., Tapponnier, P., 1975. Cenozoic tectonics of Asia: effects of a continental collision. *Science* 189 (4201), 419–426.
- Murphy, M.A., Yin, A., Harrison, T.M., Dürr, S., Chen, Z., Ryerson, F.J., et al., 1997. Did the Indo-Asian collision alone create the Tibetan plateau? *Geology* 25 (8), 719–722.
- Nelson, K.D., Wnjin, Z., Brown, L.D., Kuo, J., Jinkai, C., Xianwen, L., Klemper, S.L., Makovsky, Y., Meissner, R., Mechie, J., Kind, R., Wenzel, F., Ni, J., Nabelek, J., Leshou, C., Handong, T., Wenbo, W., Jones, A.G., Booker, J., Unsworth, M., et al., 1996. Partially molten middle crust beneath southern Tibet: synthesis of Project INDEPTH initial results. *Science* 274, 1684–1688.
- Nikolaeva, K., Gerya, T., Marques, F.O., 2010. Subduction initiation at passive margins: numerical modeling. *J. Geophys. Res.* 115, <http://dx.doi.org/10.1029/2009JB006549>.
- Nironen, M., 1997. The Svecofennian orogen: a tectonic model. *Precambrian Res.* 86, 21–44.
- Northrup, C.J., Royden, L.H., Burchfiel, B.C., 1995. Motion of the Pacific plate relative to Eurasia and its potential relation to Cenozoic extension along the eastern margin of Eurasia. *Geology* 23 (8), 719–722.
- Peltzer, G., Tapponnier, P., 1988. Formation and evolution of strike-slip faults, rifts, and basins during the India-Asia collision: an experimental approach. *J. Geophys. Res.* 93, 15085–15117.
- Peltzer, G., Tapponnier, P., Cobbold, P., 1982. The major strike-slip faults of eastern Asia – evolution and comparison with an experimental model. *Comptes rendus des séances de l'Académie des Sciences Paris Série D* 294, 1341–1348.
- Priestley, K., Jackson, J., McKenzie, D., 2008. Lithospheric structure and deep earthquakes beneath India, the Himalaya and southern Tibet. *Geophys. J. Int.* 172 (1), 345–362.
- Ranalli, G., 1995. Rheology of the Earth, Deformation and Flow Processes in Geophysics and Geodynamics. Chapman & Hall.
- Replumaz, A., Guillot, S., Villasenor, A., Negro, M., 2013. Amount of Asian lithospheric mantle subducted during the India/Asia collision. *Gondwana Res.* vol24, 936–945.
- Replumaz, A., Tapponnier, P., 2003. Reconstruction of the deformed collision zone between India and Asia by backward motion of lithospheric blocks. *J. Geophys. Res.: Solid Earth* 108 (B6).
- Ricard, Y., Richards, M., Lithgow-Bertelloni, C., Le Stuenff, Y., 1993. A geodynamic model of mantle density heterogeneity. *J. Geophys. Res.* 98, 21895–21909.
- Rongjun, Z., Yong, L., Densmore, A.L., Ellis, M., Yulin, H., Yongzhao, L., Xiaogang, L.I., 2007. Active tectonics of the Longmen Shan region on the eastern margin of the Tibetan plateau. *Acta Geol. Sin. (Engl. Ed.)* 81 (4), 593–604.
- Royden, L., 1996. Coupling and decoupling of crust and mantle in convergent orogens: implications for strain partitioning in the crust. *J. Geophys. Res.: Solid Earth* 101 (B8), 17679–17705.
- Royden, L., Burchfield, B.C., King, R.W., Wang, E., Chen, Z., Shen, F., Liu, Y., 1997. Surface deformation and lower crustal flow in Eastern Tibet. *Science* 276.
- Royden, L., Burchfield, B.C., van der Hilst, R.D., 2008. The geological evolution of the Tibetan Plateau. *Science* 321, 1054–1058.
- Schaeffer, A.J., Lebedev, S., 2013. Global shear speed structure of the upper mantle and transition zone. *Geophys. J. Int.* ggt095.

- Schellart, W.P., 2005. Influence of the subducting plate velocity on the geometry of the slab and migration of the subduction hinge. *Earth Planet. Sci. Lett.* 231 (3), 197–219.
- Schellart, W.P., Lister, G.S., 2005. The role of the East Asian active margin in widespread extensional and strike-slip deformation in East Asia. *J. Geol. Soc.* 162 (6), 959–972.
- Schmalholz, S.M., Medvedev, S., Lechmann, S.M., Podladchikov, Y., 2014. Relationship between tectonic overpressure, deviatoric stress, driving force, isostasy and gravitational potential energy. *Geophys. J. Int.* 197 (2), 680–696.
- Schoenbohm, L.M., Burchfield, B.C., Liangzhong, C., 2006. Propagation of surface uplift, lower crustal flow, and Cenozoic tectonics of the southeast margin of the Tibetan Plateau. *Geology* 34 (10), 813–816.
- Sibuet, J.C., Hsu, S.K., Debayle, E., 2004. Geodynamic context of the Taiwan orogen. In: *Continent–Ocean Interactions Within East Asian Marginal Seas*, pp. 127–158.
- Sol, S.A., Meltzer, R., Bürgmann, R.D., Van der Hilst, R.D., King, R., Chen, Z., Koons, P.O., Lev, E., Liu, Y.P., Zeitler, P.K., Zhang, X., Zhang, J., Zurek, B., 2007. Geodynamics of the southeastern Tibetan Plateau from seismic anisotropy and geodesy. *Geology* 5 (6), 563–566.
- Sternai, P., Jolivet, L., Menant, A., Gerya, T., 2014. Driving the upper plate surface deformation by slab rollback and mantle flow. *Earth Planet. Sci. Lett.* 405, 110–118.
- Tamaki, K., 1992. Tectonic synthesis and implications of Japan Sea ODP drilling. *Proc. ODP Sci. Results* 127, 1333–1348.
- Tapponnier, P., Molnar, P., 1977. Active faulting and tectonics of China. *J. Geophys. Res.* 82, 2905–2930.
- Tapponnier, P., Peltzer, G., Armijo, R., 1986. On the mechanics of the collision between India and Asia. In: Coward, M.P., Ries, A.C. (Eds.), *Collision Tectonics*, pp. 115–157.
- Tapponnier, P., Peltzer, G., Le Dain, A.Y., Armijo, R., Cobbold, P., 1982. Propagating extrusion tectonics in Asia: new insights from simple experiments with plasticine. *Geology* 10, 611–616.
- Tapponnier, P., Zhiqin, X., Roger, B., Meyer, B., Arnaud, N., Wittlinger, G., Jingsui, Y., 2001. Oblique stepwise rise and growth of the Tibet plateau. *Science* 294 (5547), 1671–1677.
- Taylor, S.R., McLennan, S.M., 1995. The geochemical evolution of the continental crust. *Rev. Geophys.* 33, 241–265.
- Turcotte, D.L., Schubert, G., 2002. *Geodynamics*. Cambridge University Press, Cambridge.
- van der Hilst, R., Seno, T., 1993. Effects of relative plate motion on the deep structure and penetration depth of slabs below the Izu-Bonin and Mariana island arcs. *Earth Planet. Sci. Lett.* 120 (3), 395–407.
- Wüstefeld, A., Bokelmann, G.H., Barruol, G., Montagner, J.P., 2009. Identifying global seismic anisotropy patterns by correlating shear-wave splitting and surface waves data. *Phys. Earth Planet. Int.* 176 (3–4), 198–212.
- Wang, E., Burchfiel, B.C., Royden, L.H., Liangzhong, C., Jishen, C., Wenxin, L., Zhilian, C., 1998. Late Cenozoic Xianshuihe–Xiaojiang, Red River, and Dali fault systems of southwestern Sichuan and central Yunnan, China. *Geol. Soc. Am. Spec. Pap.* 327, 108.
- Wang, P., Scherler, D., Liu-Zeng, J., Mey, J., Avouac, J.P., Zhang, Y., Shi, D., 2014. Tectonic control of Yarlung Tsangpo gorge revealed by a buried canyon in Southern Tibet. *Science* 346, 978–981.
- Wang, Q., Zhang, P., Freymueller, J.T., Bilham, R., Larson, K.M., Lai, X., You, X., Niu, Z., Wu, J., Li, Y., Liu, J., Yang, Z., Chen, Q., 2001. Present-day crustal deformation in China constrained by global positioning system measurements. *Science* 194.
- Willett, S., Beaumont, C., Fullsack, P., 1993. Mechanical model for the tectonics of doubly vergent compressional orogens. *Geology* 21 (4), 371–374.
- Williams, H., Turner, S., Kelley, S., Harris, N., 2001. Age and composition of dikes in Southern Tibet: new constraints on the timing of east–west extension and its relationship to postcollisional volcanism. *Geology* 29 (4), 339–342.
- Windley, B.F., 1995. *The Evolving Continents*. J Wiley & Sons, Chichester, 526 pp.
- Xu, L., Rondenay, S., van der Hilst, R.D., 2007. Structure of the crust beneath the southeastern Tibetan Plateau from teleseismic receiver functions. *Phys. Earth Planet. Inter.* 165 (3), 176–193.
- Yang, Y., Zheng, Y., Chen, J., Zhou, S., Celyan, S., Sandvol, E., Tilmann, F., Priestley, K., Hearn, T.M., Ni, J.F., Brown, L.D., Ritzwoller, M.H., 2010. Rayleigh wave phase velocity maps of Tibet and the surrounding regions from ambient seismic noise tomography. *Geochem. Geophys. Geosyst.* 11 (8).
- Zeitler, P., Meltzer, A., Koons, P., Hallett, B., Chamberlain, P., Kidd, W.S., Park, S.K., Seeber, L., Bishop, M., Shroder, J., 2001. Erosion, Himalayan geodynamics and the geomorphology of metamorphism. *GSA Today* 11.1, 4–9.
- Zhang, Z.K., Wang, M., Gan, W., Bürgmann, R., Wang, Q., Niu, Z., Sun, J., Wu, J., Han-rong, S., Xinzhaoy, Y., 2004. Continuous deformation of the Tibetan Plateau from global positioning system data. *Geology* 32, 809–812.